

# Bremsstrahlung in electron scattering by xenon

É. T. Verkhovtseva, E. V. Gnatchenko, B. A. Zon, A. A. Nekipelov, and A. A. Tkachenko

*Voronezh State University; Low-Temperature Physics and Engineering Institute, Ukrainian Academy of Sciences*

(Submitted 4 January 1990; resubmitted 21 April 1990)

Zh. Eksp. Teor. Fiz. **98**, 797–807 (September 1990)

We have studied experimentally and theoretically the x-ray emission generated by electrons scattering from xenon in the vicinity of the giant photoabsorption resonance due to the  $4d$  subshell. We have detected in the x-ray emission spectrum a pronounced maximum that resembles the photoabsorption maximum. The position of the emission maximum, however, depends on the energy of the scattered electrons and the angle between an electron's velocity vector and the direction of the emitted x ray. The phenomenon is ascribed to polarization bremsstrahlung.

## 1. INTRODUCTION

According to our best theoretical understanding,<sup>1</sup> bremsstrahlung resulting from the scattering of a charged particle by a target particle (atom or ion) can come about in two ways. The first is the emission of photons by the incoming charged particle as it slows down in the static field of the target particle—the standard “direct” bremsstrahlung channel. Such processes lead to a smooth distribution of bremsstrahlung photons, and are well-understood in terms of the commonly adopted Bethe–Heitler and Sauter theory of bremsstrahlung.<sup>2,3</sup> The screening approximation is employed in that theory to take the structure of the target particle into account: the electron clouds of atoms or ions are replaced by their electrostatic field.

There is another mechanism for producing bremsstrahlung, however. In essence, photons in the continuous spectrum are emitted not by the scattered particle, as in the first mechanism, but by the electrons of the target particle when the latter are polarized by the field of the incoming particle. The radiation produced in this way has been called “polarization” bremsstrahlung. In contrast to the Bethe–Heitler theory, target electrons are treated here as a dynamical system with internal degrees of freedom, and they play more of a role than simply statically screening the nucleus. Recent theoretical analyses<sup>1</sup> have shown that there are a number of instances in which results can differ significantly when one makes appropriate allowance for the electron shell of the target atoms or ions. The difference can amount to a modification of the frequency or angular dependence of the bremsstrahlung, and the probability of emission can become independent of the mass of the incoming particle. In contrast to conventional bremsstrahlung, the frequency dependence of polarization bremsstrahlung is not monotonic—essentially reproducing the behavior of the dynamic polarizability of the target particle—and it contributes most to that range of the spectrum where the dynamic polarizability of the target is greatest.<sup>1</sup>

It should be pointed out here that polarization bremsstrahlung has made it possible in recent years to account for a broad range of experimental facts that has heretofore defied explanation by the Bethe–Heitler theory. These include the laser-induced breakdown of alkali-metal vapors,<sup>4</sup> the appearance of giant maxima in the spectrum emitted by rare-earth and transuranic metals bombarded with fast electrons,<sup>5–7</sup> the high-intensity x rays that result when solid-

state targets are illuminated by fast protons,<sup>8</sup> and others as well.

Polarization bremsstrahlung in gases was first observed directly in dedicated experiments<sup>9</sup> involving 0–6-keV electrons scattering from Xe; the scattering occurred near the ionization threshold of the  $4d$  subshell, where there is a giant resonance in the photoabsorption spectrum of xenon.<sup>10</sup> The bremsstrahlung was manifested as a broad band whose structure resembled that of the photoabsorption peak (see Ch. 7 of Ref. 1). The polarization bremsstrahlung maximum, however, was displaced toward much higher photon energies (typically by 17 eV) than the photoabsorption peak, a result that stimulated further detailed experimental and theoretical investigations of bremsstrahlung arising from the scattering of electrons by xenon at various energies. The present paper is concerned with the results of those studies.

## 2. EXPERIMENTAL SETUP AND MEASUREMENT TECHNIQUE

A detailed investigation of the bremsstrahlung resulting from atomic scattering of electrons requires that we identify an approach capable of studying bremsstrahlung in its pure form, i.e., without adding the characteristic lines emitted by the atomic target to the bremsstrahlung spectrum. The present authors employed one such approach—the use of a supersonic jet of gas in vacuum as a dense atomic target. In fact, that approach enables one to place the electron beam in immediate proximity to the target and study the ultrasoft x-ray spectrum of isolated atoms over a wide range of incident electron energy—in other words, to systematically probe the atom with an electron beam, from the valence subbands to the innermost shells. The latter circumstance makes it possible to arrange for experimental conditions conducive to the study of bremsstrahlung—particularly in the range of photon energy over which the dynamic polarizability of the atomic target is large—under clean conditions, with no interfering atomic lines.

The experimental setup is shown in Fig. 1; it consists of an x-ray tube with a supersonic gas jet as an anode, and an RSM-500 spectrometer/monochromator.<sup>11</sup> We may describe the principle of operation as follows. The gas to be studied is injected into the heat exchanger (1) from a high-pressure vessel. Reaching the temperature of the heat exchanger, the gas is formed into a supersonic jet (9) by a conical nozzle (2), whereupon it enters a vacuum chamber.

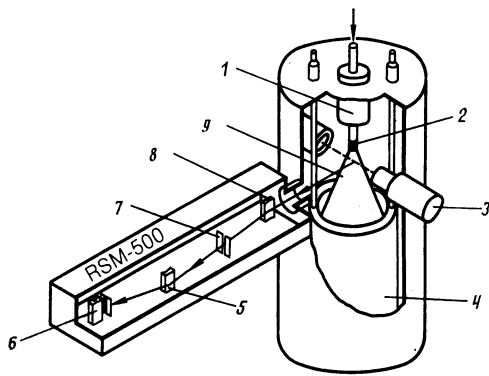


FIG. 1. Experimental setup.

The nozzle has a critical cross section of 0.38 mm (diameter), and the ratio of emergent to critical areas is 35.4. The gas from the jet is evacuated by a cryogenic pump (4) cooled with liquid hydrogen. Because of the relatively well-defined boundaries of the supersonic gas flow in vacuum ( $10^{-3}$  Pa), the electron beam (3) may be placed 40 mm from the jet, forming a beam with energy ranging from 100 to 2000 eV and a current density of 0.1 to 1 A/cm<sup>2</sup>. The electron beam traverses the jet 5 mm from the end of the nozzle and perpendicular to the nozzle axis. The resultant radiation is focused by a spherical mirror (8) onto the input slit (7) of the RSM-500 spectrometer/monochromator; it is then broken up into a spectrum by a two-meter, gold-coated concave diffraction grating (5) ruled at 600 lines/mm, and detected by an SRPP-203 proportional counter (6) filled with methane at a pressure of  $1.5 \cdot 10^4$  Pa. The window of the counter is a sheet of nitrocellulose film. The angle between the incident electrons and the photons being analyzed is 97°.

We investigated the xenon spectrum in the energy range 80–220 eV. The following considerations dictated the choice of experimental conditions.

1. The 80–220-eV energy range had to be free of interfering atomic lines of Xe. The experiments were carried out at incident electron energies of 0.3 to 0.9 keV, making it possible to avoid ionization of the 3*d* subshell of Xe and the multiline spectra in the energy range of interest that this would entail.<sup>12</sup>

2. The gas temperature and pressure at the nozzle input were chosen so as to ensure a monatomic jet with minimal bremsstrahlung self-absorption, while keeping the radiative intensity high enough in the energy range of interest. These requirements led us to choose a gas pressure  $3 \cdot 10^4$  Pa, and a temperature 650 K. The atomic number density in the beam-traversal region was  $6 \cdot 10^5$  cm<sup>-3</sup>. Under these circumstances, self-absorption of the radiation by Xe atoms is at most 5%.

In comparing the experimental spectra with theoretical predictions, it is important that one know the true shape of the spectrum. In our own work, we took into account distortions imposed on the spectrum by the efficiency of the RSM-500 spectrometer. The efficiency was determined from the ratio of the bremsstrahlung intensity from a beam of electrons scattered by an atomic jet of Ar as measured behind the exit slit of the spectrometer to the true (calculated) distribution. The bremsstrahlung spectrum from the Ar jet was obtained at an input gas pressure of  $4 \cdot 10^5$  Pa and an electron beam energy of 1 keV. The effective thickness of the gas-jet

anode was then 1.8 nm. The self-absorption coefficient was at most 2%.

In the 80–220 eV photon energy range (wavelength range  $\Delta\lambda = 15.5$ –5.5 nm), the bremsstrahlung spectrum showed virtually no lines due to Ar atoms. Since the focusing mirror and the grating (radius of curvature  $R = 2$  m) filtered out radiation at shorter wavelengths than 7–8 nm, the Ar bremsstrahlung spectrum was also free of overlapping higher diffraction orders in the wavelength range of interest. Inasmuch as the Ar jet constituted a thin anode,<sup>13</sup> we determined the true intensity distribution of the bremsstrahlung spectrum from the jet using the results of a quantum-mechanical calculation of the bremsstrahlung spectrum of just such an anode,<sup>14</sup> which are in good agreement with experimental data (Ref. 15).<sup>11</sup> The true bremsstrahlung intensity from an Ar jet at a radiation pick-off angle  $\beta$  is given by<sup>14</sup>

$$I(\beta) = I_x \sin^2 \beta + I_y (1 + \cos^2 \beta),$$

where  $I_x$  and  $I_y$  are the components of the bremsstrahlung spectrum parallel and perpendicular to the electron beam. The error in determining the instrumental efficiency is at most 10%.

Under the foregoing jet-flow conditions, and for electron-beam energies of 0.3, 0.6, and 0.9 keV, we recorded spectra at least 10 times. Since the proportional counter measures the number of photons per unit wavelength,  $N_\lambda d\lambda$ , and not the number of photons per unit frequency,  $N_\omega d\omega$ , a comparison of the experimental spectra  $N_\lambda$  with the theoretical  $N_\omega$  requires an additional normalizing coefficient:  $N_\omega = \lambda^2 N_\lambda$ . The spectra obtained were also corrected for the instrumental sensitivity of the RSM-500. The accuracy of the relative spectral intensity determination was 10%.

### 3. RESULTS OF MEASUREMENTS

In Fig. 2, we have plotted the photoabsorption spectrum of Xe in the vicinity of the 4*d* ionization threshold, and the bremsstrahlung spectrum obtained from 0.3-, 0.6-, and 0.9 keV electrons scattering from Xe atoms. An analysis of these results indicates that the bremsstrahlung spectrum recorded at fixed electron-beam energy is quite different from the spectrum predicted by the Bethe–Heitler theory. In fact, instead of a horizontal straight line in the plot of  $\omega d\sigma/d\omega d\chi$ , we observe a very broad emission band with a pronounced maximum, and structure reminiscent of the giant resonance in the photoabsorption spectrum. The observed band is comprised of polarization bremsstrahlung, and is produced via the excitation of Xe to the continuous spectrum above the 4*d* ionization threshold.<sup>9</sup>

Analysis of the spectra makes it possible to identify features engendered by the change in energy of the scattered electrons. The clearest such feature is the progressive displacement of the bremsstrahlung spectrum toward lower photon energy as the electron energy increases from 0.3 to 0.9 keV—the maximum in the experimental bremsstrahlung spectrum approaches the resonance peak of the photoabsorption spectrum. As the electron beam energy rises, the shape of the spectrum also changes: the asymmetry in the emission band tends to favor lower photon energies. Furthermore, at incident electron energies of 0.3 and 0.6 keV, the bremsstrahlung spectrum exhibits an additional maxi-

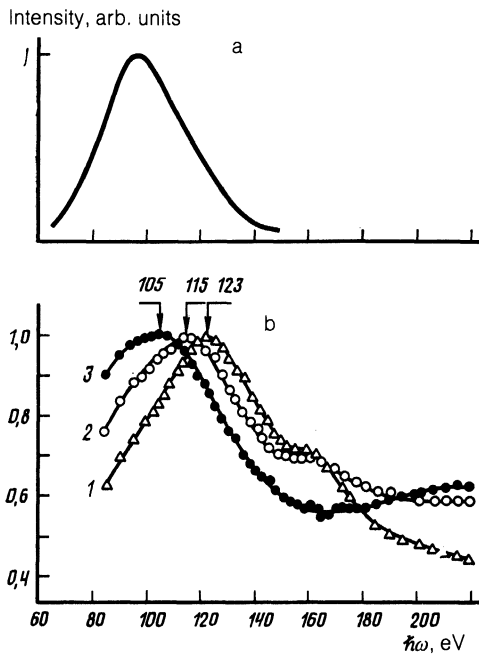


FIG. 2. Spectra: a) Xe photoabsorption; b) bremsstrahlung from electrons scattered by Xe, with incident electrons energies of 0.3 (curve 1), 0.6 (curve 2), and 0.9 (curve 3) keV. Each of the spectra has been normalized to its maximum value.

mum somewhat above the ionization threshold of the  $4d$  subshell of Xe.

#### 4. DISCUSSION

The experimental data imply that the location of the maximum in the spectrum emitted by electrons scattered from Xe atoms depends on the initial electron energy. In this section we undertake to explain that fact, invoking special considerations.

The photon energy at the maximum of the bremsstrahlung spectrum (Fig. 2) is determined by the position of the resonance peak in the photoabsorption spectrum of the  $4d$  electrons of Xe, and is only a factor of 3 to 9 lower than the initial energy of the incoming electrons; this is why the appropriateness of the Born approximation for a quantitative description of the phenomenon is dubious. The Born approximation is useful, however, in clarifying the reason why the maximum shifts as the electron energy changes, and in providing a qualitative description of that phenomenon. Moreover, the calculations below demonstrate that over the energy and frequency ranges in question, multiparticle effects due to the electronic structure of Xe and associated with the "thawing" of the crystal lattice are extremely important. Therefore, even though certain multielectron effects in atomic scattering of electrons have been taken in account in the past (e.g., see Ref. 16), it would be unwise to count on being able to deal with these effects fully in the near future—in other words, to calculate scattering cross sections much more accurate than those given by the Born approximation.

The theoretical work described in Ref. 1 deals mainly with polarization bremsstrahlung integrated over a range of directions. Differential spectra have been studied in Ref. 17, but the results obtained there do not suit our present pur-

poses. We therefore now present the appropriate derivations.

In the Born approximation, the conventional bremsstrahlung amplitude  $M_e$  and the polarization bremsstrahlung amplitude  $M_a$  may be written in the form (see Ch. 10 of Ref. 1)

$$M_e = 4\pi e^3 (2\pi\hbar\omega)^{1/2} \frac{(\mathbf{e}_{\mathbf{k}\mu}\mathbf{q})}{m\omega^2 q^2} [Z - F(\mathbf{q})], \quad (1)$$

$$M_a = \frac{4\pi e^2}{q^2} (2\pi\hbar\omega)^{1/2} \alpha_s(\mathbf{q}, \omega) \mathbf{e}_{\mathbf{k}\mu}.$$

Here  $\omega$ ,  $\mathbf{k}$ , and  $\mu$  are the frequency, wave vector, and polarization of the emitted photon,  $\mathbf{e}_{\mathbf{k}\mu}$  is a polarization unit vector,  $Z$  is the charge on the atomic nucleus,  $\mathbf{q} = \mathbf{p}' - \mathbf{p}$  is the momentum transfer of the scattered electron, and

$$F(\mathbf{q}) = \langle 0 | \sum_{i=1}^Z \exp(-i\mathbf{q}\mathbf{r}_i/\hbar) | 0 \rangle \quad (2)$$

is the atomic form factor, which in the Born approximation is determined by the elastic scattering amplitude. The index  $s$  takes on three values in the expression for  $M_a$  corresponding to Cartesian coordinates, and these are assumed to be summed over. The expression

$$\alpha_s(\mathbf{q}, \omega) = i \sum_n \left\{ \frac{1}{\omega_{n0} - \omega} \langle 0 | d_s | n \rangle \langle n | \sum_{i=1}^Z \exp(-i\mathbf{q}\mathbf{r}_i/\hbar) | 0 \rangle + \frac{1}{\omega_{n0} + \omega} \langle 0 | \sum_{i=1}^Z \exp(-i\mathbf{q}\mathbf{r}_i/\hbar) | n \rangle \langle n | d_s | 0 \rangle \right\} \quad (3)$$

is a generalization of the atomic polarizability corresponding to frequency  $\omega$  and momentum transfer  $\mathbf{q}$ , and  $\mathbf{d}$  is the atomic dipole moment operator. The summation in (3) is carried out over all virtual states of the atom, including the continuous spectrum.

In the Born-Bethe approximation, which is easily satisfied in the theory of inelastic electron-atom collisions, the exponential appearing in the matrix element in (3) may be replaced by a dipole term, so that (see Ref. 1)

$$\alpha_s(\mathbf{q}, \omega) = \frac{1}{e} \alpha_{st}(\omega) q' \Theta(\theta_a - \theta). \quad (4)$$

Here  $e$  is the electron charge,  $\alpha_{st}$  is the conventional dynamic polarizability tensor of the atom,  $\theta$  is the electron scattering angle, and  $\Theta(\cdot)$  is the Heaviside step function, which makes allowance for the fact that at scattering angles  $\theta > \theta_a \approx v_a/v \ll 1$ , the Born-Bethe approximation no longer holds, since at those angles the appropriate matrix elements are exponentially small. In the above inequalities,  $v$  is the velocity of the scattered electron and  $v_a$  is the typical velocity of the atomic electrons.

For spherically symmetric atomic states—including the ground state of Xe—the dynamic polarizability tensor reduces to a scalar:

$$\alpha_{st}(\omega) = \alpha(\omega) \delta_{st}. \quad (5)$$

Substituting (3)–(5) into (1), we obtain

$$M_a = \frac{4\pi e}{q^2} (2\pi\hbar\omega)^{1/2} (\mathbf{e}_{\mathbf{k}\mu}\mathbf{q}) \alpha(\omega) \Theta(\theta_a - \theta). \quad (6)$$

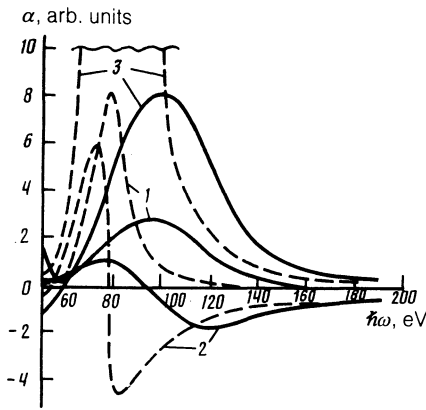


FIG. 3. Calculated dynamic polarizability of the ground state of Xe obtained using the relativistic local electron-density functional. 1)  $\text{Im } \alpha(\omega)$ ; 2)  $\text{Re } \alpha(\omega)$ ; 3)  $|\alpha(\omega)|^2$ . The solid curves have been obtained using the renormalized electromagnetic field vertex, and the dashed curves without it.

In addition, the form factor  $F(\mathbf{q})$  for symmetric states depends solely on the modulus of  $\mathbf{q}$ , a fact we shall take advantage of below.

The approximations employed here and below to derive the analytic equations are useful in illustrating the numerical calculations, which are of interest in their own right. The calculations have been carried out in a time-dependent formalism using the relativistic local electron-density functional<sup>18</sup> (all atomic electrons are taken into account), in which correlation effects are treated phenomenologically.<sup>19,20</sup>

In Fig. 3 we show the calculated dynamic polarizability of the ground state of Xe over the frequency range in which we measured bremsstrahlung. The maximum of the imaginary part of the polarizability clearly lies at 96 eV, which is rather close to the photoabsorption peak at 98 eV. Note that when we fail to take into account self-consistency effects in the electron functions in a variable external field, the agreement of the maximum of the imaginary part of the polarizability (78 eV) with experiment is much poorer. Renormalization of the vertices has just as strong an effect on the real part, and consequently on the absolute value of the polarizability, which as we shall soon see, determines the polarization bremsstrahlung spectrum. All of these effects attest to the important role played by correlation effects in Xe, which we have already remarked upon.

In Fig. 4, we have plotted the calculated generalized polarizability  $\alpha_z(q, \omega)$  as a function of  $q$  for  $\hbar\omega = 110$  eV. For the plot, we have divided the polarizability by  $q$ , since that is the quantity that enters into the integral that determines the polarization bremsstrahlung [see Eq. (7)]. The dashed curves in Fig. 4 give the Born-Bethe approximation for three incoming electron energies. Because of the presence of the Heaviside step function, the quantity of interest is discontinuous. For these calculations we have taken  $v_a = 1$  in atomic units. Naturally, it is not possible to specify the precise value of  $v_a$ , but the result ultimately depends on  $v_a$  only logarithmically, so the dependence is extremely weak. The Born-Bethe approximation is clearly quite satisfactory, and the discrepancy with the more accurate result only shows up at large  $q$ , with no effect on the value of the integral. The dash-dot curve in Fig. 4 represents the form factor

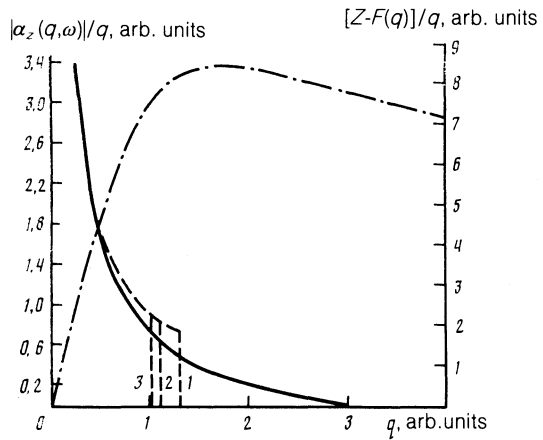


FIG. 4. Generalized dynamic polarizability of the ground state of the Xe atom (solid curve) and the corresponding Born-Bethe approximation at various incoming electron energies: 1)  $E_{e_i} = 0.3$ , 2) 0.6, 3) 0.9 keV, all with  $\hbar\omega = 110$  eV. The dot-dash curve is the Xe ground-state form factor. Calculated using the relativistic local electron-density functional.

$[Z - F(q)]/q$ , which determines the amplitude of conventional bremsstrahlung (1), as a function of momentum transfer  $q$ .

We now turn to the calculation of the total bremsstrahlung cross section. Making use of Eq. (1) for  $M_e$  and Eq. (6) for  $M_a$ , and summing over the polarizations of the emitted photons, it is straightforward to obtain an expression for the differential cross section:

$$d\sigma(\mathbf{p}', \mathbf{k}) = \frac{e^2}{\pi^2 \hbar c^3 \omega} \frac{p'}{p} \left[ 1 - \frac{(\mathbf{k}\mathbf{q})^2}{k^2 q^2} \right] \left| \frac{e^2}{q} [Z - F(q)] + \frac{m\omega^2}{q} \alpha(\omega) \Theta(\theta_a - \theta) \right|^2 d\Omega_{\mathbf{p}'} d\Omega_{\mathbf{k}} d\omega. \quad (7)$$

Here  $d\Omega_{\mathbf{p}'}$  and  $d\Omega_{\mathbf{k}}$  are the elements of solid angle corresponding to the appropriate radius vectors.

It can be seen from Fig. 4 that the first and second terms of the absolute value in Eq. (7) are sharply peaked at different values of  $q$ , and therefore at different scattering angles  $\theta$ . Interference between those terms can therefore be neglected in integrating over  $d\Omega_{\mathbf{p}'}$ ; this is justified in terms of the applicability of the Born approximation in Ref. 1.

Integrating (7) over  $d\Omega_{\mathbf{p}'}$ , then, we have

$$d\sigma(\chi, \omega) = d\sigma_e(\chi, \omega) + d\sigma_a(\chi, \omega),$$

$$d\sigma_e(\chi, \omega) = \frac{2e^6}{\pi \hbar c^3} \frac{p'}{p} \frac{d\omega}{\omega} \sin \chi d\chi \int_0^\pi \left[ \frac{Z - F(q)}{q} \right]^2 \times \left\{ 1 - \frac{1}{q^2} \left[ p'^2 \left( \cos^2 \chi \cos^2 \theta + \frac{1}{2} \sin^2 \chi \sin^2 \theta \right) - 2pp' \cos \theta \cos^2 \chi + p^2 \cos^2 \chi \right] \right\} \sin \theta d\theta,$$

$$d\sigma_a(\chi, \omega) = \frac{\alpha}{2\pi v^2 c^2} |\omega^2 \alpha(\omega)|^2 \left\{ \left[ \left( 1 - \frac{p'^2}{p^2} \right) \times \sin^2 \chi + 2 \left( 1 + \frac{p'^2}{p^2} \right) \cos^2 \chi \right] \times \ln \left( \gamma \frac{v^2}{\omega^2 R_a^2} \right) - \left( 1 + \frac{p'}{p} \right)^2 \left( \cos^2 \chi - \frac{1}{2} \sin^2 \chi \right) \right\} \frac{d\omega}{\omega} \sin \chi d\chi. \quad (8)$$

Here  $\alpha = e^2/\hbar c \approx 1/137$ ,  $\chi$  is the angle between  $\mathbf{p}$  and  $\mathbf{k}$ ,

$R_a \approx \hbar/mv_a$  is the characteristic size of the atom's electron shell, and  $\gamma$  is a factor of order unity, which is uncertain to the extent that  $\theta_a$  is. Equation (8) makes clear the fact that the cross section is independent of the azimuthal angle between  $\mathbf{k}$  and  $\mathbf{p}$ , a result of the axial symmetry of scattering from a spherically symmetry target. We have not integrated over the azimuthal angle in (8).

Integrating (8) over  $d\chi$  and multiplying that result by  $2\pi$  (for the azimuthal factor), we obtain the well-known expressions for the total bremsstrahlung cross section.<sup>1</sup> In the process, however, a very important term disappears from  $d\sigma_a$ , which contains to logarithmic factor.

The conventional bremsstrahlung cross section  $d\sigma_e$  calculated for the incoming experimental electron energies and angles  $\chi$  is a very smooth function, varying with frequency of the emitted photon by 10% at most. The displacement of the bremsstrahlung spectral peak can therefore not be related to  $d\sigma_e$ , and from here on we concern ourselves solely with an analysis of the polarization bremsstrahlung cross section  $d\sigma_a$ . To simplify the derivation, we expand the cross section in the parameter  $\varepsilon \equiv m\hbar\omega/p^2 \ll 1$ , and obtain

$$\frac{d\sigma_a(\chi, \omega)}{\sin \chi d\chi} = \frac{\alpha}{\pi v^2 c^2} |\omega^2 \alpha(\omega)|^2 \left\{ [\varepsilon \sin^2 \chi + 2(1+\varepsilon) \cos^2 \chi] L - 2(1-\varepsilon) \left( \cos^2 \chi - \frac{1}{2} \sin^2 \chi \right) \right\} \frac{d\omega}{\omega}, \quad L = \ln \left( \gamma \frac{v^2}{\omega^2 R_a^2} \right). \quad (9)$$

In particular, for  $\chi = \pi/2$ ,

$$\frac{d\sigma_a(\pi/2, \omega)}{d\chi} = \frac{\alpha}{\pi v^2 c^2} |\omega^2 \alpha(\omega)|^2 (1+\varepsilon L) \frac{d\omega}{\omega}. \quad (10)$$

For the experimental value  $\chi = 97^\circ$ ,  $\cos^2 \chi / \sin^2 \chi \approx 0.015$ , which is much less than the experimental value of  $\varepsilon$ . Equation (10) therefore provides a completely satisfactory approximation to Eq. (9).

It is clear from Fig. 3 that in the neighborhood of the maximum,  $|\alpha(\omega)|^2$  is quite symmetric, so it can be represented by a Lorentzian:

$$|\alpha(\omega)|^2 = \alpha_0^2 \frac{\omega_0^2}{(\omega - \omega_0)^2 + \Gamma^2}. \quad (11)$$

In this expression,  $\omega_0$  determines the position of the maximum, and  $\Gamma$  is the halfwidth of the curve of  $|\alpha(\omega)|^2$ . An analysis of Fig. 3 yields theoretical values  $\hbar\omega_0 = 100$  eV and  $\Gamma = 24$  eV. The frequency  $\omega_{\max}$  corresponding to the maximum cross section  $\omega d\sigma_a/d\chi d\omega$  can easily be obtained by inserting (11) into (10).

Neglecting the frequency dependence of  $L$  and assuming  $\omega_{\max} = \omega_0 + \nu$ ,  $\nu \ll \omega_0$ , we have

$$\nu = \frac{2\Gamma^2}{\omega_0} \frac{1+5\varepsilon L/4}{1+[1-5(\Gamma/\omega_0)^2/2]\varepsilon L}. \quad (12)$$

We see from Eq. (12) that as the energy of the incoming electron rises ( $\varepsilon \rightarrow 0$ ),  $\omega_{\max} \rightarrow \omega_0 + 2\Gamma^2/\omega_0$ . Thus, even in the asymptotic Born limit, the position of the polarization bremsstrahlung maximum differs, in general, from the position of the photoabsorption maximum, and the greater the width of the photoabsorption peak, the greater the difference. The difference stems basically from the fact that photoabsorption is determined by the imaginary part of the dy-

TABLE I.

$E$ , keV	$\hbar\omega_{\max}$ , eV	
	Exp.	Theor.
0,3	123±2	126
0,6	115±2	114
0,9	105±2	113

amic polarizability of the atom, and polarization bremsstrahlung by its absolute magnitude. The factor  $\omega^4$  in the polarization bremsstrahlung also plays somewhat of a role.

For  $\varepsilon \rightarrow 0$ , the foregoing theoretical values of  $\omega_0$  and  $\Gamma$  yield  $\hbar\nu \approx 11$  eV. As a result, we obtain  $\hbar\omega_{\max} \approx 111$  eV, which is several times greater than the experimental value of  $\hbar\omega_{\max}$ , even for  $E_{el} = 0.9$  keV. Nevertheless, it is clear from Table I that Eq. (12) faithfully conveys the sense in which  $\omega_{\max}$  varies with electron energy, and even the order of magnitude of that variation. In calculating the parameter  $L$  in Eq. (12), we have taken  $\omega = \omega_0$ ,  $\gamma = 1$ , and  $R_a = 0.2 \cdot 10^{-8}$  cm. The latter quantity characterizes the size of the  $4d$  shell of Xe, which is of the utmost importance in the present case.

It is possible to improve the agreement between theory and experiment by treating  $\omega_0$  and  $\Gamma$  as adjustable parameters, thereby cancelling some of the errors inherent in the local-density functional method. Such a procedure is of dubious value, however, when the interaction between the atom and incoming electron is calculated in the first Born approximation.

## 5. CONCLUSION

The experimental and theoretical results detailed above lead us to the following conclusion.

1. The fact that the bremsstrahlung spectrum near the giant photoabsorption peak for electrons scattering from Xe is not monotonic is in fact due to polarization bremsstrahlung, confirming the result obtained in Ch. 7 of Ref. 1. The dispersion relations for photoionization and bremsstrahlung are in agreement, but there is still an important difference—the maxima occur at different places in the dispersion curves. In the asymptotic Born limit, this distinction is basically due to the probability of ionization being determined by the imaginary part of the atom's dynamic polarizability, while the probability of polarization bremsstrahlung is due to the absolute value. In that limit, the difference between the peak frequencies vanishes only for very narrow resonance lines, for which the real part of the dynamic polarizability can be neglected in comparison with the imaginary.

2. For differential spectra of polarization bremsstrahlung, the position of the maximum on the dispersion curve, away from the asymptotic Born limit, depends on the incoming electron energy. The direction and rate of change of that maximum with electron energy is related to the angle between the electron velocity vector and the wave vector of the emitted bremsstrahlung photon.

It should also be noted that the Born approximation and the calculations of atomic characteristics have been carried out using the relativistic local electron-density functional, which provides a satisfactory description of the experimentally observed location of the maxima of the

bremsstrahlung dispersion curves. The discrepancy between theory and experiment amounts to no more than a few percent here, although the theoretical curve departs the asymptotic regime before it conforms to the experimental curve. Here we must again stress that in the theory, there is not a single additional adjustable parameter, compared with the widely adopted local electron-density method.

The calculated dynamic polarizability of Xe shows no anomalies at all where additional irregularities in the experimental bremsstrahlung spectra appear, a fact discussed at the end of Section 2. Further studies are therefore required to clarify the nature of those features.

The authors thank M. Ya. Amus'ya, V. M. Buimistrov, and V. N. Tsytovich for discussions and useful comments.

<sup>1)</sup> According to Ref. 7, the contribution of polarization bremsstrahlung in the photon-energy range 80–220 eV for electrons scattered by Ar atoms is small.

<sup>1</sup> M. Ya. Amus'ya, V. M. Buimistrov, B. A. Zon, *et al.*, *Polarization Bremsstrahlung of Particles and Atoms* [in Russian], Nauka, Moscow (1987).

<sup>2</sup> H. Bethe and W. Heitler, *Proc. R. Soc.* **146**, 83 (1934).

<sup>3</sup> F. Sauter, *Ann. Phys.* **9**, 217 (1931).

<sup>4</sup> J. E. Rizzo and R. C. Klewe, *Brit. J. Appl. Phys.* **17**, 1137 (1966).

<sup>5</sup> T. M. Zimkina, A. S. Shulakov, and A. P. Braiko, *Fiz. Tverd. Tel.* **23**, 2006 (1981).

<sup>6</sup> T. M. Zimkina, I. I. Lyakhovskaya, A. S. Shulakov *et al.*, *Fiz. Tverd. Tel.* **25**, 26 (1983).

<sup>7</sup> M. Ya. Amus'ya, T. M. Zimkina, and M. Yu. Kuchiev, *Zh. Tekh. Fiz.* **52**, 1424 (1982) [*Sov. Phys. Tech. Phys.* **27**, 866 (1982)].

<sup>8</sup> K. Ishii and S. Morita, *Phys. Rev.* **A30**, 2278 (1984).

<sup>9</sup> E. T. Verkhovtseva, E. V. Gnatchenko, and P. S. Pogrebnyak, *J. Phys.* **B16**, L613 (1983).

<sup>10</sup> R. Haensel, G. Keitel, P. Schreiber, and G. Kung, *Phys. Rev.* **188**, 1375 (1969).

<sup>11</sup> E. T. Verkhovtseva and P. S. Pogrebnyak, *X-Ray Analysis: Instruments and Methods* [in Russian], Mashinostroenie, Leningrad (1980).

<sup>12</sup> E. T. Verkhovtseva and P. S. Pogrebnyak (Pogrebnyak), *J. Phys.* **B13**, 358 (1980).

<sup>13</sup> P. S. Pogrebnyak, Yu. A. Pavlenko, E. T. Verkhovtseva *et al.*, *Prib. Tekh. Eksp.* (1974)

<sup>14</sup> P. Kirkpatrick and L. Weidmann, *Phys. Rev.* **67**, 321 (1945).

<sup>15</sup> T. J. Peterson and D. H. Tomboulion, *Phys. Rev.* **125**, 235 (1962).

<sup>16</sup> N. B. Avdonina and M. Ya. Amus'ya, *Zh. Tekh. Fiz.* **53**, 341 (1983) [*Sov. Phys. Tech. Phys.* **28**, 209 (1983)].

<sup>17</sup> J. Ya. Amus'ya, N. B. Avdonina, M. Yu. Kuchiev, and L. V. Chernysheva, *Izv. Akad. Nauk SSSR, Ser. Fiz.* **50**, 1261 (1986).

<sup>18</sup> D. A. Liberman and A. Zangwill, *Comput. Phys. Comm.* **32**, 75 (1984).

<sup>19</sup> S. Lundqvist and N. H. March (eds.), *Theory of Inhomogeneous Electron Gas*, Plenum, New York (1983).

<sup>20</sup> S. A. Zapryagaev and A. V. Mogilev, *Opt. Spektrosk.* **59**, 730 (1985) [*Opt. Spectrosc. (USSR)* **59**, 441 (1985)].

Translated by Marc Damashek